ChemComm

COMMUNICATION

View Article Online
View Journal

Cite this: DOI: 10.1039/c8cc09688k

Received 6th December 2018,
Accepted 4th January 2019

DOI: 10.1039/c8cc09688k

rsc.li/chemcomm

Substrate-free and label-free electrocatalysis-assisted biosensor for sensitive detection of microRNA in lung cancer cells†

Lin Cui,‡[a] Meng Wang,‡[a] Bing Sun,*[b] Shiyun Ai,[c] Shaocong Wang[a] and Chunyang Zhang*[a]

We develop a substrate-free and label-free electrocatalysis-assisted biosensor for sensitive detection of microRNA using the iron-embedded nitrogen-rich carbon nanotubes (FeCN) as the catalytic elements. This biosensor exhibits excellent selectivity and high sensitivity with a detection limit of 8.53 × 10^{-16} M and a large dynamic range of 6 orders of magnitude. It can be further applied for accurate quantification of microRNA in lung cancer cells.

The development of efficient biosensors for sensitive and rapid detection of biomarkers is essential for early clinic diagnosis. Recently, the electrochemical biosensors have attracted more and more attention due to their low cost, good flexibility, high sensitivity, rapidity, and portability.[1–3] The performance of electrochemical biosensors relies on both the generation of electrochemical signal and the electron transfer on the electrode interfaces. To improve the assay performance, some electrocatalysts such as noble metals (*e.g.*, Pd,[4] Pt,[5] and Au[6]), metal oxides (*e.g.*, MnO_2,[7] Fe_3O_4,[8] and CeO_2[9]) and carbon-based nanomaterials[10] have been introduced to achieve an amplified signal. Despite the good electrocatalytic performance of noble metal-based mimetic catalysts, their widespread applications are limited by their low earth-abundance and high cost.[11–13] Alternatively, great efforts have been put into the development of inexpensive electrocatalysts with earth-abundant elements.[14]

The noble-free metal (*e.g.*, Fe, Co, Ni)–N–C materials are usually prepared by pyrolyzing separate metal, nitrogen and carbon precursors,[15] and they have the balanced surface wettability and the low-valence metal species, exhibiting high activity and good selectivity at low over-potential for electrochemical oxygen reduction reaction (ORR)[16,17] and electrochemical reduction of CO_2.[18] Despite their improved activities and durabilities,[16,18–22] the preparation of highly active metal–N–C catalysts usually involve the harsh synthetic conditions and the complicated synthesis routes. In this research, we demonstrate the facile and scalable synthesis of iron-embedded nitrogen-rich carbon nanotubes (FeCN) by simple thermal treatment and their application in the construction of electrochemical biosensor for microRNA assay.

The conventional electrocatalysis-assisted electrochemical biosensors usually rely on the H_2O_2-mediated peroxidase catalytic reactions with the characteristics of instability and easy decomposition of externally H_2O_2,[23–27] resulting in a limited detection sensitivity. Consequently, the development of stable substrate-free electrocatalysis-assisted electrochemical biosensors is highly desirable. Recently, Zhu group[28] demonstrated the construction of an electrochemical cytosensor for circulating tumor cells assay based on the electrocatalysis of redox molecules by Fe_3O_4@Pd–Ag hybrid particles without the involvement of H_2O_2. Wang *et al.*[29] reported the fabrication of an electrochemical aptasensor for ochratoxin A assay based on the substrate-free electrocatalysis of thionines by NH_2-Co-MOF. To the best of our knowledge, there is no report about the label-free and substrate-free electrocatalysis-assisted microRNA biosensor so far.

In this research, we demonstrate for the first time the development of a label-free and substrate-free electrocatalysis-assisted microRNA biosensor with FeCN as the catalytic element and the electroactive thionine as the signal reporter.[28,29] The FeCN enables the electrocatalysis reduction of thionine in the absence of H_2O_2, and the introduction of abundant thionines greatly enhances the electrochemical signal. The principle of substrate-free and label-free electrocatalysis-assisted biosensor for microRNA assay is shown in Scheme 1. The precursor Fe^{2+}-*g*-C_3N_4 is prepared in one-step self-assembly of inexpensive starting materials including dicyandiamide and $FeCl_2{\cdot}4H_2O$ (Scheme 1A). The one-step synthesis of FeCN can be achieved by simple thermal treatment

[a] College of Chemistry, Chemical Engineering and Materials Science, Collaborative Innovation Center of Functionalized Probes for Chemical Imaging in Universities of Shandong, Key Laboratory of Molecular and Nano Probes, Ministry of Education, Shandong Provincial Key Laboratory of Clean Production of Fine Chemicals, Shandong Normal University, Jinan 250014, China. E-mail: cyzhang@sdnu.edu.cn; Fax: +86-531-82615258; Tel: +86-531-86186033

[b] School of Science, China University of Geosciences (Beijing), Beijing 100183, China. E-mail: sunbing@cugb.edu.cn; Tel: +86-10-82322758

[c] College of Chemistry and Material Science, Shandong Agricultural University, Taian 271018, China

† Electronic supplementary information (ESI) available: Details of experimental procedures and additional figures. See DOI: 10.1039/c8cc09688k

‡ These authors contributed equally to this work.

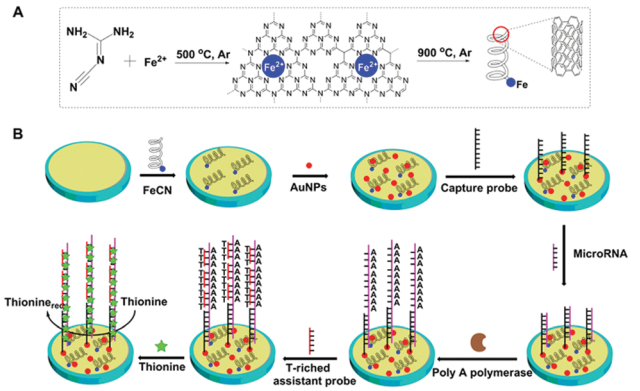

Scheme 1 Schematic illustration of the substrate-free and label-free electrocatalysis-assisted biosensor for microRNA assay. (A) The preparation of FeCN; (B) construction of the electrocatalysis-assisted biosensor for microRNA assay.

of Fe^{2+}-functionalized graphitic carbon nitride (Fe^{2+}-*g*-C_3N_4) at 900 °C in Ar atmosphere. The construction of electrochemical biosensor is illustrated in Scheme 1B. The thiolated capture probes are immobilized on the FeCN- and AuNP-modified GCE electrode by layer-by-layer self-assembly *via* the Au–S bond. Then the capture probes hybridize with the target microRNAs, and the resultant surface-bound microRNAs are subsequently polyadenylated at the 3′-OH termini by poly(A) polymerase to form the poly(A) tails which can further hybridize with the T-rich assistance probes to form the double-stranded DNAs (dsDNAs). At last, many redox molecules (*i.e.*, thionine) can be efficiently intercalated into the dsDNA grooves, and the FeCN modified on the electrode can catalyze thionines to generate an enhanced electrochemical signal without the involvement of any unstable substrate H_2O_2.

We used XRD to investigate the crystalline structure of FeCN catalyst (Fig. 1A). The peak at 26.2 °C represents the characteristic diffraction of carbon(002) plane, in agreement with the structural feature of CNTs.[30] The peaks at 40–50 °C can be indexed to the diffraction of Fe_3C structure[31] (JCPDF No. 89-2867), indicating the formation of FeCN after the thermal polycondensation and carbonization.[32] Fig. 1B shows a typical TEM image of the synthesized FeCN with a few Fe nanoparticles (Fig. 1B, red circle) being inserted in FeCN. The diameter of FeCN is in the range of 20–30 nm. In the high-resolution TEM image (Fig. 1C), a significant layer space of 0.35 nm is observed, corresponding to the stacking space of graphitic carbon. The degree of graphitization of FeCN is further investigated by Raman spectrum whose D band (1360 cm^{-1}) and G band (1590 cm^{-1}) may provide information about the disorder and crystallinity of sp^2 carbon materials. As shown in Fig. 1D, the I_D/I_G is 0.91, indicating a high degree of graphitization[20] due to the formation of a carbon tube microstructure which facilitates the improvement of electrical conductivity.[19] We further performed XPS analysis to investigate the surface nature of FeCN. Based on the survey XPS spectrum of FeCN (see ESI,† Fig. S1), C, O, N and Fe are clearly observed without any other impurities, consistent with the result of XRD (Fig. 1A). Moreover, the energy dispersive X-ray spectroscopy (EDX) (see ESI,† Fig. S2) and the elemental mapping (see ESI,† Fig. S3) verify the existence of C, O, N and Fe in FeCN. A high-resolution N1s XPS spectrum (Fig. 1E) shows the existence of pyridinic, pyrrolic and graphitic N in FeCN. The XPS spectra of Fe2p shows the presence of two photoelectron peaks at 711.1 and 724.9 eV (Fig. 1F), corresponding to the binding energies of $Fe2p_{3/2}$ and $Fe2p_{1/2}$, respectively, indicating the existence of Fe^0.[20]

We used cyclic voltammograms (CV) and different pulse voltammetry (DPV) to investigate the electrocatalysis of thionines by FeCN (Fig. 2). As shown in Fig. 2A, a bare GCE exhibits a pair of well-defined redox peaks at −0.108 V and −0.142 V (Fig. 2A, curve a) due to the reversible reduction and oxidation of thionines. When the FeCN is modified on the glassy carbon electrode (GCE), the cathodic peak current significantly increases, with the peak potential shifting from −0.142 V to −0.169 V (Fig. 2A, curve b), demonstrating the high electrocatalytic activity of FeCN towards thionines. In addition, the results of DPV (Fig. 2B) are consistent with those of CVs (Fig. 2A). The value of ΔI is 10.28 μA (the change of DPV responses ΔI is given by $\Delta I = I - I_0$, where the bare GCE is recorded as I_0 and the FeCN-modified GCE is recorded as I). The current of thionines obtained from the FeCN-modified GCE (12.30 μA) is much higher than that obtained from the bare GCE (2.022 μA). Unlike the natural horseradish peroxidase (HRP)[33,34] and the peroxidase mimetics based on nanomaterials (*e.g.*, metallic,[35] bimetallic nanostructures,[36] metal oxides and binary compounds[37]), the FeCN can electrocatalyze the reduction of

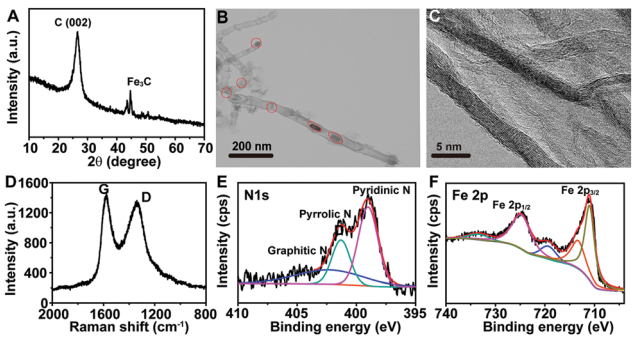

Fig. 1 (A–C) XRD pattern (A), TEM (B) and high-resolution TEM (C) images of the synthesized FeCN. (D) Raman spectrum of FeCN. (E and F) High-resolution N1s XPS spectra (E) and Fe2p XPS spectra (F) of FeCN.

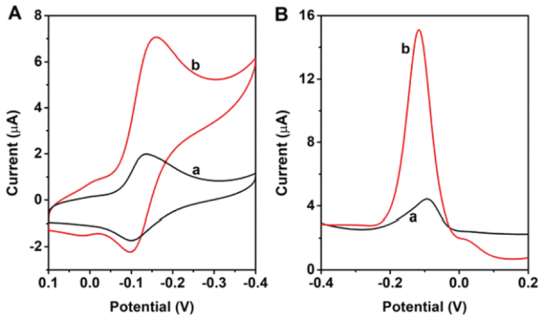

Fig. 2 CV (A) and DPV (B) curves of bare GCE (a) and FeCN-modified GCE (b) in response to the electrocatalysis of 35 μM thionine in 0.1 M HAc–NaAc solution (pH 5.0).

thionines without the involvement of any unstable H_2O_2, with a much higher ΔI obtained from the FeCN-modified electrode (10.28 μA) than that obtained from HRP/H_2O_2-modified electrode (6.25 μA).[29]

We further investigated the CV curves of thionines obtained from bare GCE and FeCN/GCE with different scan rate (see ESI,† Fig. S4). The obtained peak current is proportional to the square root of scanning rate ($\nu^{1/2}$), indicating the diffusion-controlled electrocatalytical reduction of thionines on the surface of FeCN. The plot of i_{pc} *vs.* $\nu^{1/2}$ of the FeCN-modified GCE shows a steep slope compared with that of the bare GCE, further verifying the catalytic role of FeCN in the electrochemical reduction of thionines. In addition, the CV and electrochemical impedance spectra (EIS) indicate that the assembled biological macromolecule layers may block the electron transfer (see ESI,† Fig. S5).

Under the optimally experimental conditions (see ESI,† Fig. S6), we investigated the sensitivity of the proposed biosensor. As shown in Fig. 3A, the DPV signal enhances with the increasing concentration of microRNA from 0.001 to 1000 pM, with a good linear relationship being obtained between the variation of DPV current and the logarithm of microRNA concentration ranging from 1 fM to 1000 pM with a correlation coefficient of 0.9966 (Fig. 3B). The corresponding equation is $\Delta I = 0.829 \log_{10} C + 2.754$, where ΔI is the current difference (defined as $\Delta I = I - I_0$, where I_0 and I are the DPV current of the modified electrode before and after incubation with microRNA, respectively) and C is the microRNA concentration (pM). The detection limit is calculated to be 8.53×10^{-16} M based on 3 times standard deviation over the blank response, superior to those of the reported methods for microRNA assay[38–48] (see ESI,† Table S2). The high sensitivity may be ascribed to the high electrocatalytical activity of FeCN[19] and the efficient signal amplification induced by both poly(A) polymerase-catalyzed amplification and the introduction of abundant redox molecules (*i.e.*, thionines).[49]

We used the complementary target microRNA-486-5p and the mismatched microRNA including single-base mismatched strand and three-base mismatched strand to investigate the selectivity of the proposed electrochemical biosensor. As show in Fig. 4, a high electrochemical signal is obtained in response to the complementary target microRNA-486-5p, with the change of DPV peak current being 5.35-fold higher than that in response to the single-base mismatched strand and 9.47-fold higher than that in response to the three-base mismatched strand. In addition, this electrochemical biosensor exhibits excellent stability and good reproducibility (see ESI,† Fig. S7).

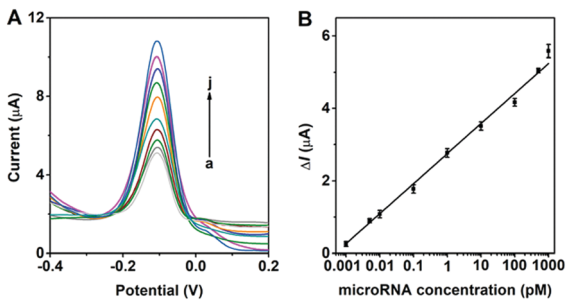

Fig. 3 (A) Electrochemical DPV curve of the biosensor incubated with different concentrations of microRNA (from a to j: 0, 0.001, 0.005, 0.01, 0.1, 1, 10, 100, 500, 1000 pM). (B) Linear relationship between the current difference (ΔI) and the logarithm of microRNA concentration in the range from 0.001 to 1000 pM. The ATP concentration is 1.0 mM, and the concentration of poly(A) polymerase is 10 U mL^{-1}. Error bars represent the standard deviation of three independent experiments.

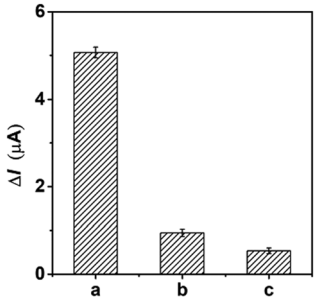

Fig. 4 Selectivity of the biosensor toward 100 pM target microRNA-486-5p (a), 100 pM single-base mismatched strand (b) and 100 pM three-base mismatched strand (c). Error bars represent the standard deviation of three independent experiments.

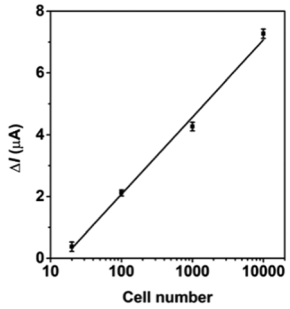

Fig. 5 Linear correlation between the current difference (ΔI) and the logarithm of A549 cell number in the range from 20 to 10 000 cells. Error bars represent the standard deviations of three independent experiments.

To investigate the feasibility of the proposed biosensor for real sample analysis, we measured the endogenous microRNA in total RNA samples extracted from human lung adenocarcinoma cells (A549 cells) which were purchased from Cell Bank of Chinese Academy of Sciences (Shanghai, China).[50] The cells were processed by a RNA extraction kit after cell counting. Notably, in logarithmic scale, the peak current difference exhibits a linear correlation with the number of cells in the range from 20 to 10 000 cells (Fig. 5). The linear equation is $\Delta I = 2.504 \log_{10} X - 2.937$ ($R^2 = 0.9914$), where X is the number of A549 cells and ΔI is the current change. The detection limit is determined to be 2 cells based on 3 times standard deviation over the blank response. Moreover, the results obtained by the proposed electrochemical biosensor (Fig. 5) are consistent with those obtained by quantitative-reverse transcription PCR (qRT-PCR) (see ESI,† Fig. S8). These results clearly demonstrate that this biosensor can be used for accurate quantification of microRNA in real biological samples.

In conclusion, we have developed a substrate-free and label-free electrocatalysis-assisted biosensor for sensitive detection of

microRNA using FeCN as the catalytic element and the electroactive thionine as the signal reporter. This electrocatalysis-assisted biosensor has distinct advantages: (1) this electrocatalysis-assisted biosensor is substrate-free without the involvement of any substrates,[28,29] greatly simplifying the operation procedures; (2) the FeCN can electrocatalyze thionines with higher electrocatalytical activity than HRP,[29] significantly amplifying the electrochemical signal; (3) target microRNA-directed polymerase-catalyzed formation of poly(A) DNA sequence at 3′-OH terminal does not involve either nucleic acid templates or special design of specific restriction enzyme recognition sequences; (4) the efficient intercalation of thionines into the DNA grooves eliminates the laborious labeling process, leading to both an enhanced electrochemical signal and an extremely low background signal. Importantly, this electrocatalysis-assisted biosensor can be extended to the detection of a variety of target nucleic acids by just simply changing the sequence of capture probe, with wide potential applications in biomedical research and clinical diagnosis.

This work was supported by the National Natural Science Foundation of China (Grant No. 21527811, 21735003, 21605096, and 21802128), and the Award for Team Leader Program of Taishan Scholars of Shandong Province, China.

Conflicts of interest

There are no conflicts to declare.

Notes and references

1 T.-Z. Liu, R. Hu, X. Zhang, K.-L. Zhang, Y. Liu, X.-B. Zhang, R.-Y. Bai, D. Li and Y.-H. Yang, *Anal. Chem.*, 2016, **88**, 12516–12523.
2 M. Wang, Z. Fu, B. Li, Y. Zhou, H. Yin and S. Ai, *Anal. Chem.*, 2014, **86**, 5606–5610.
3 L. Cui, J. Hu, C.-c. Li, C.-m. Wang and C.-y. Zhang, *Biosens. Bioelectron.*, 2018, **122**, 168–174.
4 C. Ge, G. Fang, X. Shen, Y. Chong, W. G. Wamer, X. Gao, Z. Chai, C. Chen and J.-J. Yin, *ACS Nano*, 2016, **10**, 10436–10445.
5 Z. Song, R. Yuan, Y. Chai, Y. Zhuo, W. Jiang, H. Su, X. Che and J. Li, *Chem. Commun.*, 2010, **46**, 6750–6752.
6 Y. Jv, B. Li and R. Cao, *Chem. Commun.*, 2010, **46**, 8017–8019.
7 J. Liu, L. Meng, Z. Fei, P. J. Dyson, X. Jing and X. Liu, *Biosens. Bioelectron.*, 2017, **90**, 69–74.
8 H. Wang, S. Li, Y. Si, Z. Sun, S. Li and Y. Lin, *J. Mater. Chem. B*, 2014, **2**, 4442–4448.
9 T. Naganuma, *Nano Res.*, 2017, **10**, 199–217.
10 Y. Hu, X. J. Gao, Y. Zhu, F. Muhammad, S. Tan, W. Cao, S. Lin, Z. Jin, X. Gao and H. Wei, *Chem. Mater.*, 2018, **30**, 6431–6439.
11 Z. Tian, C. Liu, Q. Li, J. Hou, Y. Li and S. Ai, *Appl. Catal., A*, 2015, **506**, 134–142.
12 W. Shi, H. Fan, S. Ai and L. Zhu, *RSC Adv.*, 2015, **5**, 32183–32190.
13 Y. Zhuo, P.-X. Yuan, R. Yuan, Y.-Q. Chai and C.-L. Hong, *Biomaterials*, 2009, **30**, 2284–2290.
14 N. Wang, B. Li, F. Qiao, J. Sun, H. Fan and S. Ai, *J. Mater. Chem. B*, 2015, **3**, 7718–7723.
15 S. Gupta, D. Tryk, I. Bae, W. Aldred and E. Yeager, *J. Appl. Electrochem.*, 1989, **19**, 19–27.
16 A. Zitolo, N. Ranjbar-Sahraie, T. Mineva, J. Li, Q. Jia, S. Stamatin, G. F. Harrington, S. M. Lyth, P. Krtil and S. Mukerjee, *Nat. Commun.*, 2017, **8**, 957.
17 M. Sun, D. Davenport, H. Liu, J. Qu, M. Elimelech and J. Li, *J. Mater. Chem. A*, 2018, **6**, 2527–2539.
18 W. Ju, A. Bagger, G.-P. Hao, A. S. Varela, I. Sinev, V. Bon, B. R. Cuenya, S. Kaskel, J. Rossmeisl and P. Strasser, *Nat. Commun.*, 2017, **8**, 944.
19 X. Zou, X. Huang, A. Goswami, R. Silva, B. R. Sathe, E. Mikmeková and T. Asefa, *Angew. Chem., Int. Ed.*, 2014, **53**, 4372–4376.
20 Y. Yao, H. Chen, C. Lian, F. Wei, D. Zhang, G. Wu, B. Chen and S. Wang, *J. Hazard. Mater.*, 2016, **314**, 129–139.
21 Y. Cao, B. Zhao, X. Bao and Y. Wang, *ACS Catal.*, 2018, **8**, 7077–7085.
22 Q. Ma, L. Cui, S. Zhou, Y. Li, W. Shi and S. Ai, *Environ. Sci. Pollut. Res.*, 2018, 1–8.
23 L. Cui, J. Hu, M. Wang, X.-k. Diao, C.-c. Li and C.-y. Zhang, *Anal. Chem.*, 2018, **90**, 11478–11485.
24 H. Wei and E. Wang, *Chem. Soc. Rev.*, 2013, **42**, 6060–6093.
25 Z.-H. Yang, S. Ren, Y. Zhuo, R. Yuan and Y.-Q. Chai, *Anal. Chem.*, 2017, **89**, 13349–13356.
26 X. Yang, J. Lv, Z. Yang, R. Yuan and Y. Chai, *Anal. Chem.*, 2017, **89**, 11636–11640.
27 Q. Zhang, Y. Qiao, F. Hao, L. Zhang, S. Wu, Y. Li, J. Li and X. M. Song, *Chem. – Eur. J.*, 2010, **16**, 8133–8139.
28 T. Zheng, Q. Zhang, S. Feng, J.-J. Zhu, Q. Wang and H. Wang, *J. Am. Chem. Soc.*, 2014, **136**, 2288–2291.
29 Z. Wang, H. Yu, J. Han, G. Xie and S. Chen, *Chem. Commun.*, 2017, **53**, 9926–9929.
30 X. Fan, Z. Peng, R. Ye, H. Zhou and X. Guo, *ACS Nano*, 2015, **9**, 7407–7418.
31 W. Yang, X. Liu, X. Yue, J. Jia and S. Guo, *J. Am. Chem. Soc.*, 2015, **137**, 1436–1439.
32 J. Xiang, J. Li, X. Zhang, Q. Ye, J. Xu and X. Shen, *J. Mater. Chem. A*, 2014, **2**, 16905–16914.
33 C. Ruan, F. Yang, C. Lei and J. Deng, *Anal. Chem.*, 1998, **70**, 1721–1725.
34 T. T. Zheng, J. J. Fu, L. H. Hu, F. Qiu, M. J. Hu, J. J. Zhu, Z.-C. Hua and H. Wei, *Anal. Chem.*, 2013, **85**, 5609–5616.
35 Z. J. Song, R. Yuan., Y. Q. Chai., Y. Zhuo, W. Jiang, H. L. Su, X. Che and J. J. Li, *Chem. Commun.*, 2010, **46**, 6750–6752.
36 X. Gao, R. Gui, K. Q. Xu, H. Guo, H. Jin and Z. Wang, *New J. Chem.*, 2018, **42**, 14796–14804.
37 Q. Li, L. Zeng, J. Wang, D. Tang, B. Liu, G. Chen and M. Wei, *ACS Appl. Mater. Interfaces*, 2011, **3**, 1366–1373.
38 J. Zhang, L. Chao, Z. Xiao, G. A. Ramón, Y. Liu, C. Zhang, P. Fei and D. Cui, *Anal. Chem.*, 2015, **88**, 1294–1302.
39 F. Xu, H. Shi, X. He, K. Wang, D. He, Q. Guo, Z. Qing, L. Yan, X. Ye and D. Li, *Anal. Chem.*, 2014, **86**, 6976–6982.
40 L. R. Zhang, G. Zhu and C. Y. Zhang, *Anal. Chem.*, 2014, **86**, 6703–6709.
41 X. Miao, Z. Cheng, H. Ma, Z. Li, N. Xue and P. Wang, *Anal. Chem.*, 2017, **90**, 1098–1103.
42 F. Ma, M. Liu, B. Tang and C. Y. Zhang, *Anal. Chem.*, 2017, **89**, 6182–6187.
43 T. Tian, H. Xiao, Z. Zhang, Y. Long, S. Peng, S. Wang, X. Zhou, S. Liu and X. Zhou, *Chem. – Eur. J.*, 2013, **19**, 92–95.
44 H. Wu, Y. Liu, H. Wang, J. Wu, F. Zhu and P. Zou, *Biosens. Bioelectron.*, 2016, **81**, 303–308.
45 D. Zhu, W. Liu, D. Zhao, Q. Hao, J. Li, J. Huang, J. Shi, J. Chao, S. Su and L. Wang, *ACS Appl. Mater. Interfaces*, 2017, **9**, 35597–35603.
46 N. Xia, L. Zhang, G. Wang, Q. Feng and L. Liu, *Biosens. Bioelectron.*, 2013, **47**, 461–466.
47 Y. Zhou, H. Yin, J. Li, B. Li, X. Li, S. Ai and X. Zhang, *Biosens. Bioelectron.*, 2016, **79**, 79–85.
48 Q. Tian, Y. Wang, R. Deng, L. Lin, Y. Liu and J. Li, *Nanoscale*, 2015, **7**, 987–993.
49 F. Shiping, L. Hye Jin, A. W. Wark and R. M. Corn, *J. Am. Chem. Soc.*, 2006, **128**, 14044–14046.
50 R. Deng, K. Zhang and J. Li, *Acc. Chem. Res.*, 2017, **50**, 1059–1068.

